DNS OF CONJUGATE HEAT TRANSFER IN TURBULENT CHANNEL FLOWS

Paolo Orlandi
Dipartimento di Meccanica e Aeronautica
Via Eudossiana 16, Roma Italy
orlandi@kolmogorov.ing.uniroma1.it

Stefano Leonardi
Dep. of Mech. Eng.
University of Puerto Rico at Mayaguez, Puerto Rico

Giorgio Amati
CASPUR - Via dei Tizii n.6b,Roma Italy

ABSTRACT

In real applications of heat transfer between two isothermal walls, the constant temperature is applied at the external side of the solid walls, which have a thickness and a thermal conductivity depending on the material used. Usually, in numerical simulations the solid layer is neglected and the constant temperature is assigned at the no-slip boundary. In the present simulations the Navier-Stokes equations together with four transport equations for a passive scalar, which can represent either concentration or temperature, are solved. The evolution of the passive scalars differs only for the conductivity in the solid, while the diffusivity of the fluid is the same. The Reynolds number effect has been investigated by two simulations one at $R_\tau = 180$ and the other at $R_\tau = 335$, where $R_\tau = u_\tau h/\nu$ is the friction velocity Reynolds number. Two point correlations, flow visualizations and probability density function of the thermal field have been evaluated to quantify how deeply the effect of the turbulent flow penetrates inside the solid.

INTRODUCTION

In the numerical simulations of heat transfer in turbulent channel, usually, temperature boundary conditions are assigned on the solid walls. This is a condition that does not reproduce real conditions or laboratory experiments, where the temperature is maintained constant on the external side of the walls. In these circumstances the thickness and the thermal conductivity of the wall play an important role, which, to our knowledge, has been rarely investigated by direct numerical simulations. Previous DNS, Kim & Moin (1992), at low Re numbers, and Kawamura *et al.* (2004), at high Re, were focused on the influence of the fluid Pr number. By adding a uniform volumetric heating into the scalar transport equation, as for the total velocity stress, the sum of the wall-normal turbulent and molecular heat fluxes, normalised by the wall heat flux, decreases linearly from 1 to 0 at the centerline. Without the constant heat source, the total heat flux is constant across the channel. This case was considered by Johansson & Wikstrom (1999) at $R_\tau = 180$ and 265; they analysed the issues related to the Reynolds averaging turbulence models. Orlandi & Leonardi (2004a), at $R_\tau = 180$ and 395 fixed $Pr = 1$, and validated their finite difference second order method, by comparing their results with those obtained by Johanson & Wikstrom (1999) by a pseudospectral method. In addition by adding a realistic transpiration at the solid wall they made an attempt to understand the effects of rough walls on heat transfer.

In the present simulations the same numerical method of Orlandi & Leonardi (2004a) has been used to couple the transfer of the passive scalar in the solid with that in the fluid. The immersed boundary technique described by Leonardi & Orlandi (2004b) was employed to this purpose. In presence of straight walls the method is simple due to the periodicity in two directions. A particular attention is necessary in the passive scalar equation to get a continuous heat flow at the interface between solid and fluid.

PHYSICAL AND NUMERICAL MODEL

The incompressible non-dimensional Navier-Stokes and continuity equations may be written as:

$$\frac{\partial U_i}{\partial t} + \frac{\partial U_i U_j}{\partial x_j} = -\frac{\partial P}{\partial x_i} + \Pi\delta_{i3} + \frac{1}{Re}\frac{\partial^2 U_i}{\partial x_j^2} \; ; \quad \frac{\partial U_i}{\partial x_i} = 0 \; , \quad (1)$$

where $Re = (U_c h/\nu)$ is the Reynolds number, U_c is the laminar Poiseuille centerline velocity, Π is the pressure gradient required to maintain a constant flow rate, U_i is the component of the velocity vector in the i direction, P is the pressure, x_1, x_2 and x_3 are the streamwise, wall-normal and spanwise directions; h is the half channel width. The computational domain extend in both side up to $1.2h$; in the $0.2h$ thick layers there is a conducting solid. To impose, in this layer, a zero velocity, the immersed boundary technique, described by Leonardi & Orlandi (2004b), is used. In presence of straight walls the method is very simple to insert in a code (Orlandi 2000) solving the flow with two periodic and one non homogeneous directions. Π is evaluated by a discrete integral of the RHS of the discretized streamwise momentum equations. With the method of Leonardi & Orlandi (2004b) the total mass is fully conserved. Moreover, the staggered scheme, for inviscid conditions with free-slip boundaries, in the limit of $\Delta t = 0$, for any kind of non-uniform grid in the normal direction, conserves the total kinetic energy. This requirement is important to have a stable time integration scheme.

Combined with the Navier-Stokes equations, the equation for the passive scalar $\theta = T/T_0$ is considered

$$\frac{\partial \theta}{\partial t} + \frac{\partial \theta U_j}{\partial x_j} = \frac{1}{Re\, Pr_F}\frac{\partial^2 \theta}{\partial x_j^2} \quad (2)$$

T_0 is the constant temperature at $x_2 = \pm 1.2$, with opposite sign in the two sides. Eq.(2) holds in the region with the fluid and does not require any condition at the interface between

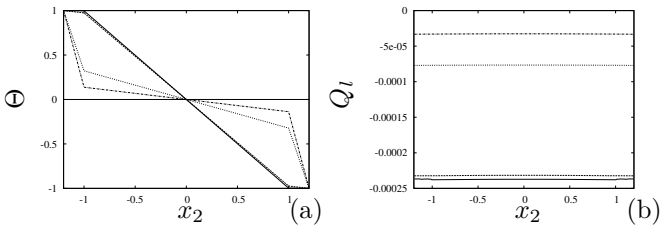

Figure 1: a) Θ, b) heat flux $Q = \alpha_i \partial\Theta/\partial x_2$ profiles varying Pr_S; solid 0.0134, dashed 0.134, dotted 10.5, dashdotted 30.8.

the fluid and the solid. In the solid layers the θ transport equation is

$$\frac{\partial \theta}{\partial t} = \frac{1}{Re\ Pr_S} \frac{\partial^2 \theta}{\partial x_j^2} \tag{3}$$

θ indicates the temperature field for each solid conductivity α_S. In the simulations the fluid Prandtl number is $Pr_F = \nu/\alpha_F = 1$. Four values for the solid Prandtl number $Pr_S = \nu/\alpha_S$ have been assumed: $0.0134, 0.134, 10.5$ and 30.8. These correspond to different materials: the first is an ideal material with a conductivity higher than copper (0.134). The last two correspond respectively to marble and glass.

The Navier-Stokes equations have been discretized in an orthogonal coordinate system using a staggered central second-order finite-difference approximation. More details of the numerical method can be found in Orlandi (2000). The discretized system is advanced in time using a fractional-step method with viscous terms treated implicitly and convective terms explicitly. The large sparse matrix resulting from the implicit terms is reduced in sparseness by FFTs in the homogeneous directions. Tridiagonal solvers in the non-homogeneous directions permit to get the solution at the new time step. The reduced wavenumber instead of the real wavenumber maintains the second-order accuracy of staggered finite differences. The same discretization and time advancement procedure is used for the passive scalar transport equations. The non-uniform grid in the x_2 direction gives a better resolution near the interface, this is obtained by two hyperbolic tangent transformations, both in the region with the fluid and with the solid. The continuity of the first derivative at the interface permits to yield the stretching parameter in the conducting layer by fixing the desired number of point in this layer and the stretching parameter in the fluid side. The number of grid points depend on the Reynolds number, while the size of the computational box is the same for the streamwise (4π) and for the spanwise (2π) directions. For the low Reynolds number the grid is $129 \times 193 \times 129$ respectively in the streamwise,normal and spanwise direction. In the normal direction 24 points are assumed for each conducting layers. The resolution of the turbulent flows is almost identical to that used in Kim *et al* (1987). At the higher Re the number of points was doubled in the homogeneous directions. The number of points in the conducting layers increased to 32 and to get, near the solid boundaries, the resolution close to that in the pseudospectral simulations, the number of points inside the channel was increased to 352. In the present simulations the resolution in wall units is smaller than that in Kim *et al* (1987), they used $256 \times 193 \times 192$ in a computational box 2π by π in the homogeneous directions. In addition the cos coordinate transformation locates the first grid point closer to the wall than the hyperbolic tangent. The DNS of turbulent channels are very sensitive to the grid points distribution near the walls then some small discrepancy between our results and the pseudospectral should be expected. In an unpublished study, it has been shown that this $2nd$ order finite difference method, with an identical resolution of the pseudospectral simulations, produces identical velocity and vorticity rms profiles.

At the interface the heat flux in the two side must be equal; numerically to reach this goal is convenient to define θ at the same location of U_2 and the diffusivities at the center of the cell. At the steady state the heat flux, across the three layers, should be constant with and without fluid motions. The stationary solution of Eq.(3) and Eq.(2) without convective terms, has been assumed as the initial condition to reach the statistically steady state in presence of fluid motion. This steady state conducting solution has a physical interest, in fact for $Pr_S = 30.8$ reproduces the insulated windows in building constructions, where the thin layer of air, between the solid walls, does not move. In Fig.1 the temperature profiles and the heat flux for the four diffusivity above mentioned are given. The dimensionless temperature in the case with fluid at rest is indicated by Θ to distinguish it from θ in presence of the flow. Fig.1a shows that for high conducting walls, the temperature decreases in the fluid layer of thickness $2h$, with $Pr = 1$. For low conducting walls, the temperature decreases in the solid. Fig.1b, from the numerical side, shows that the heat flux, as expected, is constant; from the physical side shows that for glass the heat flux is largely reduced. This solution was obtained by solving Eq.(2) and Eq.(3) in the x_2 direction with $U_i = 0$. By taking at $t = 0$ $\theta = \pm 1$ on the external walls and $\theta = 0$ elsewhere, the convergence to the steady state is faster as Pr_S is higher. By assigning the steady thermal field together with a fully developed turbulent velocity field the statistically steady state, for the thermal field, was achieved in a reduced amount of CPU time.

RESULTS

The present paper is in large part devoted to analyse the statistics related to the temperature, however it is worth to show that the statistics of the velocity components agree with those by Kim *et al.* (1987) that are considered as reference results. In the coordinate transformation it is important to find a satisfactory stretching parameter for the hyperbolic tangent. For instance when the first grid point is at $y^+ = 0.26$, the results, in the viscous region, differ from those by Kim *et al.* (1987) where the first grid point was at $y^+ = 0.05$. By changing the stretching parameter to have the first grid point at $y^+ = 0.076$ there is an improvement. Fig.2a shows a good agreement between the mean velocity profiles, in wall units. Both simulations present a downward shift of the log region, by increasing the Reynolds number. The present $R_\tau = 330$ is slightly smaller than $R_\tau = 395$ in Kim *et al.* (1987), therefore the profiles of the normal stresses can not perfectly overlap those of the pseudospectral simulations. Fig.2b shows the same $< u_1'^2 >^{+1/2}$ near the wall, but the peak values differ, in particular at high Re. This shift is due, in a reduced manner, to the different R_τ. The present simulations show a small dependence of the peaks, on Re, with respect to that found in the pseudospectral simulations. This is related to the different resolution in the homogeneous directions. Here $\Delta x_1 = 16, \Delta x_3 = 8$ while in Kim *et al.* (1987) $\Delta x_1 = 10, \Delta x_3 = 6.5$. Fig.2 indeed shows that the present numerical method produces a satisfactory turbulent flow between one heated and one cooled wall. This flow will affect the heat transfer, which

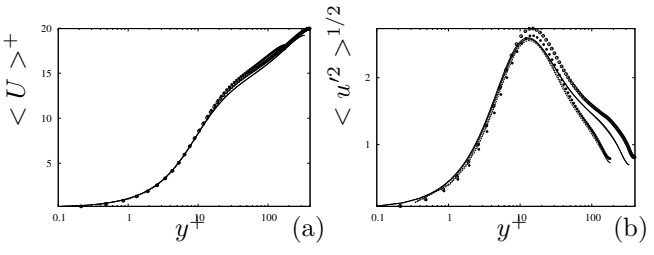

Figure 2: a) Mean velocity, b) streamwise velocity rms in wall units: solid symbols Kim *et al.* (1987), solid line high Re, dashed line low Re.

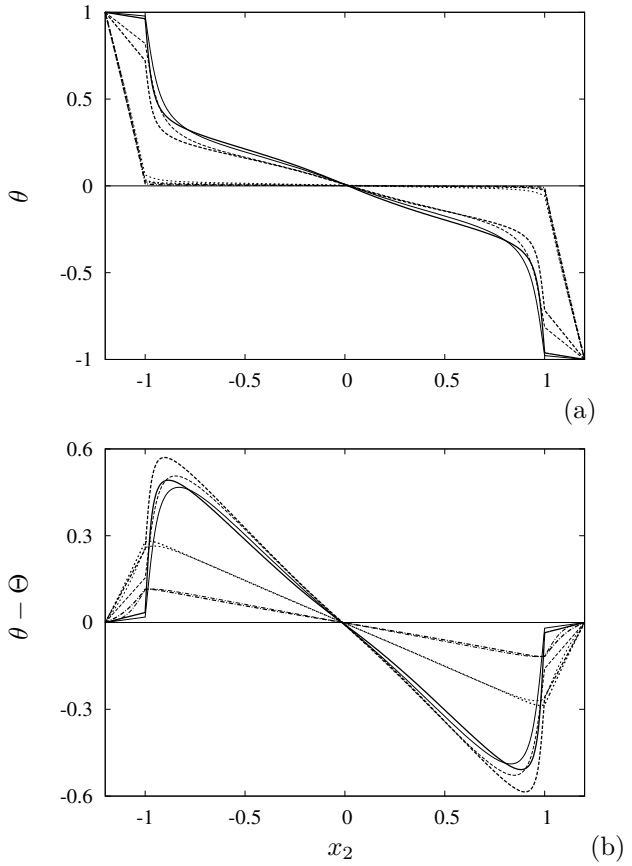

Figure 3: a) θ, b) $\theta - \Theta$ profiles varying Pr_S; solid 0.0134, dashed 0.134, dotted 10.5, dashdotted 30.8, thick lines for $R_\tau = 330$, thin lines for $R_\tau = 180$

depends also on the thermal conductivity of the solid walls. This last dependence, not often studied, is the phenomenon investigated in the present study.

Regarding the temperature rms, it has been observed a convergence, to a statistical steady state, slower than that of the velocity rms, and faster as higher is the conductivity of the solid. The statistics were evaluated by the uncorrelated fields, saved after the transient ends. By increasing the Reynolds number the number of fields needed to reach the statistical convergence increases; depending also on the order and kind of statistics. For the mean temperature profiles few fields are enough. The number increases for the normal correlations, and a greater number is needed for the correlation between temperature and velocity. This explains the small oscillations, around the expected linear profile, for some of the total heat fluxes. To eliminate the oscillations on $< \theta' u_2' >$, it is necessary to have more than the 200 fields here used.

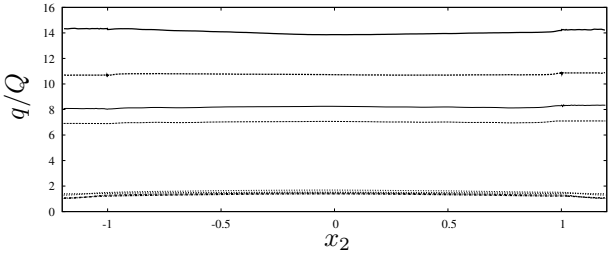

Figure 4: Normalised heat flux varying Pr_S; solid 0.0134, dashed 0.134, dotted 10.5, dashdotted 30.8, thick lines for $R_\tau = 330$, thin lines for $R_\tau = 180$

Fig.3a shows that Re number affects the mean temperature for high conducting materials, and that the greatest influence occurs for copper. For insulating materials the temperature decreases in the solid, and then the effect of the flow characteristic is negligible. To emphasize the effects of the flow characteristics is convenient to plot $\Theta - \theta$. In fact, in Fig.3a, it is difficult to appreciate the difference between marble and glass, on the other hand, in Fig.3b is clear that for glass (the most insulated material) the influence of the flow is small, and that there is no difference between the two Reynolds numbers. To understand that only in presence of turbulent flows there are changes on the heat transfer, it is important to remember that Θ is also the solution for laminar flows. This has been verified by a simulation at $Re = 1000$ with a small initial velocity perturbation, on the Poiseuille profile. It has been observed that the initial Θ profile does not change. So we can conclude that, with poorly conducting materials, the strength and the shape of the near wall vortical structures, Re dependent, do not affect the heat transfer; is important that the structures persist to weakly affect the mean temperature profiles. For high conducting materials, Fig.3b shows that with copper there is the greatest effect, and that a further increase of the conductivity brings to a decrease on $\theta - \Theta$. The evaluation of the correlations and flow visualizations permit to explain this occurrence.

The constant heat flux,

$$q = -\frac{1}{Pe}\partial\theta/\partial x_2 + < \theta' u_2' > \qquad (4)$$

increases when the flow is turbulent. In Eq.(4) $Pe = RePr_S$ in the solid layers (Pe indicates the Peclet number), and $Pe = RePr_F$ in the fluid. To quantify the effects of the turbulence is worth to normalize the heat fluxes with Q (the heat flux for laminar flow given in Fig.(1)). Fig.4 shows that for low conducting materials the heat flux at any Reynolds number remains almost constant and equal to that without motion. On the other hand, a large increase with Re occurs for high conducting materials, and this increases by increasing the thermal conductivity. It is interesting to notice that for copper at $R_\tau = 180$, the heat flux increases 7 times larger than the heat flux for laminar flow. Hamilton *et al.* (1995) found that $R_\tau = 100$ is the minimum friction Reynolds number to have the streaky structures near the wall. Even if we did not measure the heat transfer at $R_\tau = 100$; we can assume that it is close to that in a laminar regime, hence the heat transfer increases seven times by doubling Re_τ up to $R_\tau = 180$. A further doubling of Re_τ increases the heat flux respect to $Re_\tau = 180$ of a factor 11/7. A further increase of Re_τ should give a lower augmentation, therefore a limit on the heat transfer with Re_τ would exist. To find this limit, simulations at higher Re are necessary, and these will be performed in the near future.

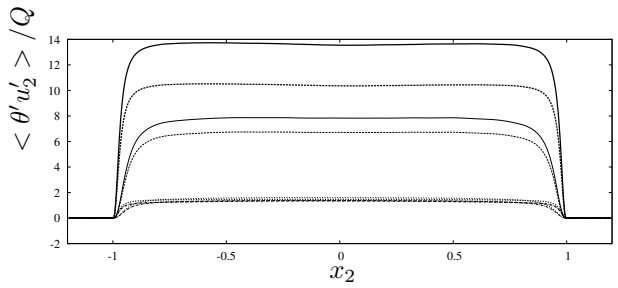

Figure 5: Normalised turbulent heat flux varying Pr_S; solid 0.0134, dashed 0.134, dotted 10.5, dashdotted 30.8, thick lines for $R_\tau = 330$, thin lines for $R_\tau = 180$

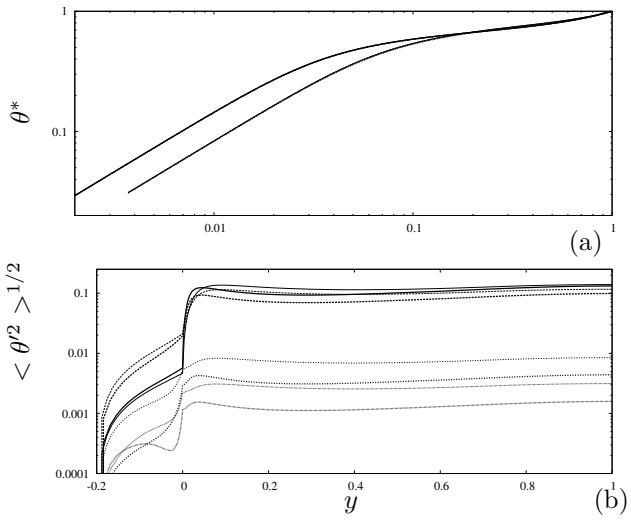

Figure 6: a) θ^* , b) $< \theta'^2 >^{1/2}$ profiles versus $y = 1 - |x_2|$ varying Pr_S; solid 0.0134, dashed 0.134, dotted 10.5, dashdotted 30.8, thick lines for $R_\tau = 330$, thin lines for $R_\tau = 180$

The turbulent contribution $< \theta' u_2' > /Q$ to the total heat flux (shown in Fig.5) is predominant in the central region of the channel. The amount due to the mean temperature gradient overcomes the turbulent flux only in the region near the wall, this term is of the same order of Q, as it can be appreciated by comparing Fig.4 and Fig.5. We would like to remind that the flat behavior of $< \theta' u_2' >$ in the central region of the channel occurs with isothermal walls and absence of heat sources.

By scaling $\theta^* = |(\theta - \theta_I)/(\theta_c - \theta_I)|$, with θ_I the temperature at the interface and θ_c that at the centerline (here $\theta_c = 0$), near the wall a linear profile, with a constant slope independent on Re, is obtained (Fig.6a). The effect of the Reynolds number is to shift upward the profile. This was also observed in channels with a fix temperature on the walls. In that set-up, also $< \theta'^2 >^{1/2}$ had a similar trend near the wall. The conjugate heat transfer gives peculiar profiles of $< \theta'^2 >^{1/2}$ in the solid and in a reduced measure near the wall. For instance in Fig.6b, for copper, the temperature fluctuations are higher than those for the highest conducting material. Despite this occurrence in the solid, the highest temperature fluctuations in the fluids are achieved at the high conductivity of the solid. Contrary to the expectations the maxima of $< \theta'^2 >^{1/2}$ are reached at low instead of high Re. This strange behavior is explained by a comparison between two-point U_1 and temperature correlations. Fig.7 shows that, near the wall, the growth of $\hat{\theta} =< \theta'^2 >^{1/2}_I - < \theta'^2 >^{1/2}_I / < \theta'^2 >^{1/2}_c - < \theta'^2 >^{1/2}_I$ increases with Re, and that the highest values are reached at

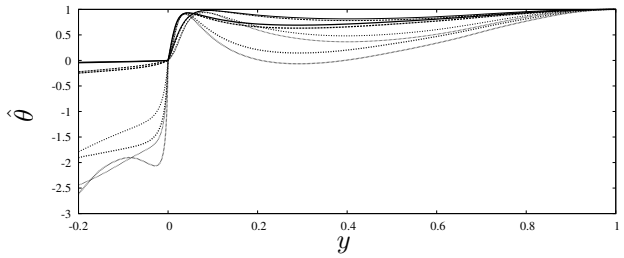

Figure 7: Normalised temperature rms varying Pr_S; solid 0.0134, dashed 0.134, dotted 10.5, dashdotted 30.8, thick lines for $R_\tau = 330$, thin lines for $R_\tau = 180$

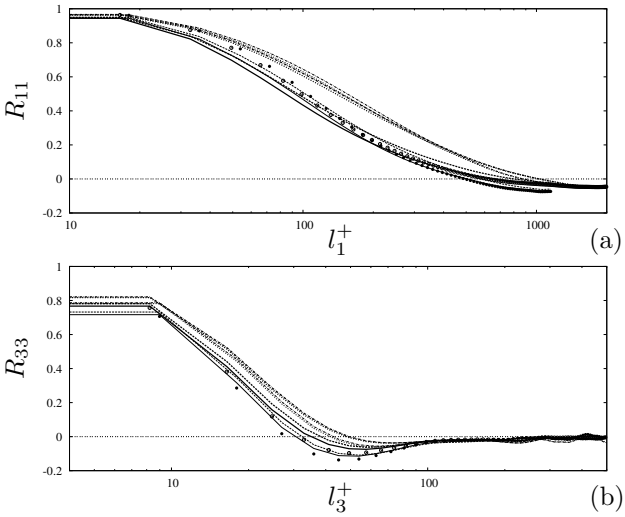

Figure 8: a) Spanwise, b) streamwise two point correlations for temperature and velocity inside the fluid at a distance $y \approx 15$ wall units: solid symbols velocity at high Re open at low Re; for temperature solid 0.0134, dashed 0.134, dotted 10.5, dashdotted 30.8, thick lines for $R_\tau = 330$, thin lines for $R_\tau = 180$

small Re. If the conductivity is low, glass for instance, the reduction of $< \theta'^2 >^{1/2}$ in the fluid leads to smaller values than those at the wall. Also this can be explained through two-point correlations or flow visualizations.

Kim & Moin (1992) by DNS obtained a strong correlation between negative values of θ' and u_1', which was, previously, postulated by the experimentalist (Kline *et al.* 1967) in the detection of the high and low speed structures by flow visualizations. This is in particular true if $Pr_F = 1$ and with a well defined source of the passive scalar. In the present simulations the near wall structures should affect the thermal fields also in the interior of the solid. It can be expected that in materials with low conductivity the influence in the solid is weak, and strong in material with high conductivity. The near wall structures are elongated in the streamwise directions (between 600 and 800 wall units) and are separated by 100 wall units, hence are closer when Re increases. Even if in the solid the wall units do not have a physical meaning the two-point correlations are plotted versus the distance in wall units, to have an immediate impression of the persistence of the shape of the high- and low-speed streaks in the solid. At a distance from the wall where there is the maximum of turbulent kinetic energy, the two-point U_1 correlations in the streamwise (Fig.8a) and in the spanwise (Fig.8b) directions, are almost independent on Re. The two-point correlations of temperature are similar to the velocity for high conducting

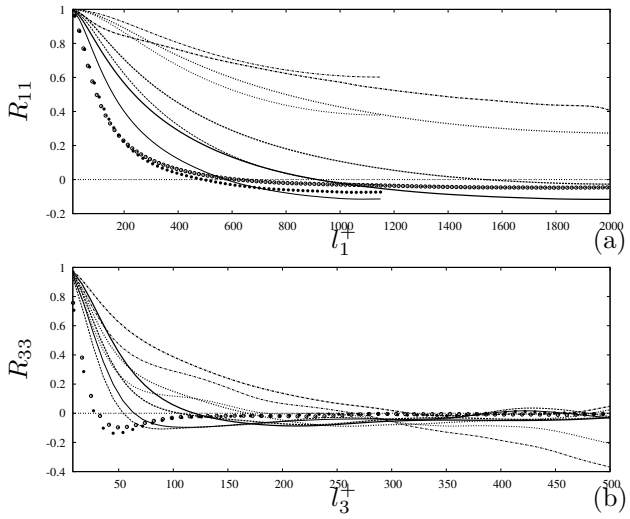

Figure 9: a) Spanwise, b) streamwise two point correlations for temperature inside the solid at a distance from the wall $y = 0.015$ compared with those of the streamwise velocity (Fig.8): solid symbols velocity at low Re open at high Re; for temperature solid 0.0134, dashed 0.134, dotted 10.5, dash-dotted 30.8, thick lines for $R_\tau = 330$, thin lines for $R_\tau = 180$

walls and low Re. On the other hand, for low conducting walls the figures show that an increase of Re leads to a reduction on the amplitude of the negative peak and to a shift toward greater distances. Fig.8a shows that at high Re and low conductivity the minimum occurs at the end of the computational box, implying that the structures are very long. This is the reason why at high Re a greater box than that in Kim *et al.* (1987) was used.

To understand how deep the effects of the near wall vortical structures penetrate in the solid, the two-point correlations of the thermal field were evaluated at a distance $y = 0.015$ from the wall, this distance is half of the distance where the correlations in Fig.8 were evaluated. Fig.9a shows that for low conducting materials the structures are much longer than the computational box. Together with Fig.9b we can assert that, for glass, there is a substantial loss of any kind of thermal field structure. With a good approximation the temperature is almost constant in the solid at a very small distance from the interface. For the marble at small Re a sensible reduction of the longitudinal correlation appears ($R_{11} = 0.4$), and a clear alternation of positive and negative thermal fluctuations is not reached. Only for very high conducting materials and at low Re the vortical structures affect the thermal field inside the solid. Fig.9b indeed shows that the size and the distance between positive and negative fluctuations is greater than that for the high- and low-speed streaks.

Flow visualizations produce a further information to understand what happens inside the solid. In Fig.10 color contours of θ' scaled with the local rms (the normalised quantities are indicated by $\tilde{q}$, i.e. $\tilde{\theta} = \theta' / < \theta^{2\prime} >^{1/2}$), are plotted at the same location where Fig.9a and Fig.9b were evaluated. Isocontours of u_1', also scaled by the local rms in the flow side at the distance of Fig.8, are superimposed. Near the wall there is a large probability to have $u_1' > 0$ associated to $u_2' < 0$ and vice-versa. So near the hot wall an ejection $u_2' > 0$ contributes to transport high temperature away from the wall into the fluid hence $\theta' > 0$. The opposite is expected for the inrush ($u_2' < 0$, $\theta' < 0$). The final result is to have in correspondence with low-speed

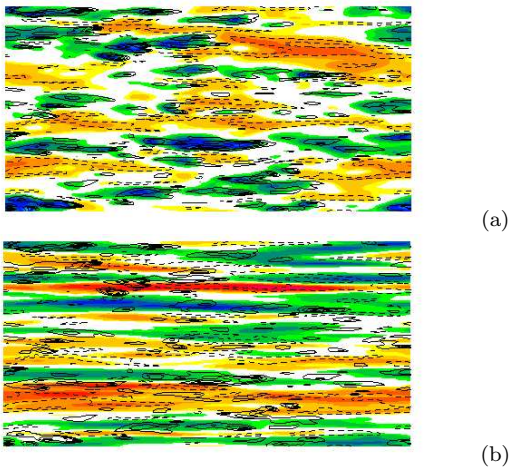

Figure 10: Flow visualizations of normalized θ' at $y = -0.015$, color contours (red yellow > 0, blue green < 0), superimposed to normalised u_1' at $y = 0.032$ (solid > 0, dashed < 0); a) $Pr_S = 0.0134$, b) $Pr_S = 30.8$.

streaks (dashed lines) hotter regions (red or yellow) and vice-versa for the high-speed streaks. It is important to notice that these visualizations are done in the side of the hot wall ($-1 < x_2 < 0$) where $\langle \theta' u_1' \rangle$ is negative. Near the opposite wall $\langle \theta' u_1' \rangle$ is positive and an opposite behavior is expected. Fig.10 shows that $\langle \theta' u_1' \rangle < 0$ for the high and low conducting walls. Fig.10, in addition clearly demonstrates that the alternate regions of positive and negative θ' are very elongated for the lowest conducting fluids. The fluctuating gradients are largely reduced and very seldom high temperature fluctuations occur. For the highest conducting solid (Fig.10a) the regions of positive and negative θ' correspond well to the low- and high-speed regions.

It is difficult to reconcile the two-point temperature correlations in Fig.9b (several fields) with the visualizations in Fig.10b (one field). Hence to understand the occurrence of strong events inside the solid and their dependence on the conductivity, the probability density functions of the quantities in the flow visualizations can be of great help. The pdf, in fact, have a clear physical meaning, being evaluated by several fields so the number of samples are greater than those in the visualizations. For instance at high Re are $N \approx 10^7$ and at low Re $N \approx 10^6$. By plotting in the same figure the pdf of $\tilde{\theta}$ and of $\tilde{u}_1$ it is possible to quantify the different occurrences of strong events. The pdf are evaluated near the hot wall at the same distance of two-point correlations and visualizations. Fig.11a shows a rather good independence on Re. $\tilde{\theta}$ and $-\tilde{u}_1$ are negatively skewed, for $\tilde{\theta}$ a small tendency toward a Gaussian distribution can be appreciated for low conducting walls. Fig.11b shows that the pdf of $\tilde{\theta}$ inside the wall is close to the velocity near the wall, only for high conducting materials. For the other materials, by decreasing the conductivity there is a reduction of the strong negative fluctuations and that the temperature is not correlated with the flow field.

In studying flow turbulence, the statistics of the derivatives rather than the statistics of the variables are of interest. In fact, only the derivatives, show non Gaussian distributions. In horizontal planes at a distance from the interface derivatives in the streamwise and spanwise directions can be evaluated, and due to the shape of the structures should have different distributions. Fig.12a shows that the velocity gradient skewness is negative ($-\partial u_1'/\partial x_1$ is plotted) and highly intermittent; with high conducting materials the correspon-

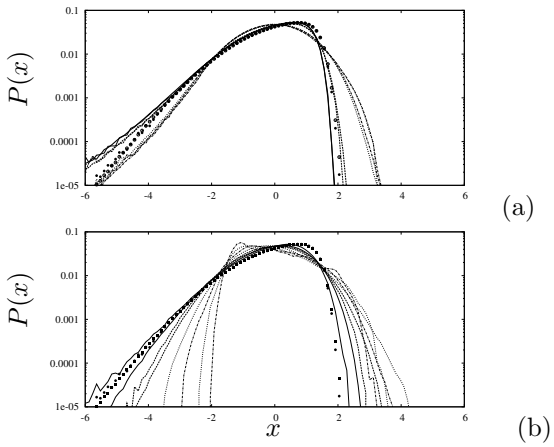

Figure 11: Probability density function of $\tilde{u}_1$ and $\tilde{\theta}$ at a) $y = 0.035$ inside the fluid, b) $y = -0.015$ inside the solid; solid symbols velocity at low Re open at high Re; for temperature solid 0.0134, dashed 0.134, dotted 10.5, dashdotted 30.8, thick lines for $R_\tau = 330$, thin lines for $R_\tau = 180$

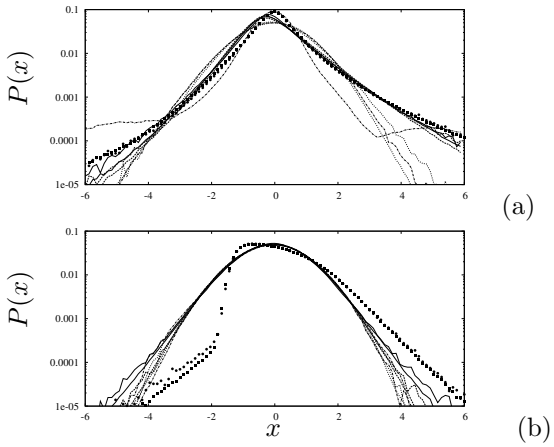

Figure 12: Probability density function of a) $\tilde{\partial} q/\partial x_1$ and $\tilde{\theta}$, b) $\tilde{\partial} q/\partial x_3$ at a) $y = -0.015$ inside the solid; solid symbols $q = u_1$ at low Re open at high Re; when q is temperature solid 0.0134, dashed 0.134, dotted 10.5, dashdotted 30.8, thick lines for $R_\tau = 330$, thin lines for $R_\tau = 180$

dence between thermal and velocity fields is a good. By reducing the conductivity the fields are less correlated. This is a sign that the fluctuating temperatures are distributed in structures much longer than those associated to the velocity distributions (symbols in the figures). For glass, at high Re, the strange shape of the pdf is related to the very small value of the rms of $\partial\theta/\partial x_1$, with a large part of points without gradients and several points where the gradients are more than twice its rms. The high intermittent character of the longitudinal derivatives is clearly shown for any quantity Fig.12a. The distribution radically change for the spanwise derivatives, it remains negative skewed (positive in Fig.12b for the velocity derivative). $\partial\theta/\partial x_3$ does not follow $\partial u_3/\partial x_3$ at all, it becomes independent on the conductivity and Re. Inside the solid the distribution is close to be Gaussian. The independence on Pr_S and on Re was found also in the fluid side near the wall, with the difference that in the fluid the distribution has quite strong tails.

CONCLUSIONS

In this study DNS of convective turbulent heat transfer demonstrate that to have results of practical interest it is important to consider also the heat transfer in the conducting materials of the walls. In these preliminary studies it has been assumed that the thickness of the wall does not vary, also this parameter plays a role. In addition there are applications where the conductivity of the two walls may be different. Several other parameters can be varied and to understand the effect of each requires an enormous amount of simulations. The most important conclusion, then, is that, the previous DNS, with the temperature assigned on the no-slip wall is quite far from the real applications, in particular for poor conducting walls. The effect of the Re number has been investigated, instead the fluid Prandtl number has been neglected. $Pr_F = 1$ is a satisfactory assumption for air. For water Pr_F is greater and hence a finer resolution is required to describe the stronger temperature gradients.

The present paper was devoted mainly to heat transfer, but the same procedure can be used to understand the mass transfer. The main application for mass transfer can be usefull for biological applications, where the passive scalars can react both in the fluid and in the tissue layers. It is not too difficult to add in the transport equations the chemical reactions, but if the reactions are stiff a particular care is needed in the time integration procedure. Despite the added difficulties this study shows that the immersed boundary technique here used is very promising.

ACKNOWLEDGMENTS

The support of a MIUR 60 % grant is aknowledged. Computational time was in large part given by CASPUR.

REFERENCES

Moin, P. & Kim, J. 1982. "Numerical investigation of turbulent channel flow number", *J. Fluid Mech.* **177**, 341–377.

Kawamura H., Abe H. Matsuo Y. 2004 "Very large-scale structures observed in DNS of turbulent channel flow with passive scalar transport", 15^{th} *Australasian Fluid Mechanics Conference, Sydney Australia.*

Johansoson A.V. & Wikstrom P.M. 1999 "DNS and modeling of passive scalar transport in turbulent channel flow with focus on scalar dissipation modeling", *Flow Turbulence and Combustion* **63**, 223–245.

Orlandi P. & Leonardi S. 2004 "Passive scalar in a turbulent channel flow with wall velocity disturbances ", *Flow Turbulence and Combustion* **72**, 181–197.

Leonardi S. & Orlandi P. 2004 "A numerical method for turbulent flows over complex geometries", *ERCOFTAC BULLETTIN* **62**:41-46.

Orlandi, P. 2000. *Fluid Flow Phenomena : A Numerical Toolkit*, Dordrecht, Kluwer.

Kim, J. , Moin, P. & Moser, R. 1987. Turbulence statistics in fully developed channel flow at low Reynolds number. *J. Fluid Mech.* **177**, 133–166.

Hamilton,J.M., Kim, J. & Waleffe, F. 1995. Regeneration mechanism of near wall turbulence structures *J. Fluid Mech.* **287**, 313–348.

Kim, J. , Moin, P. 1989. Transport of passive scalars in a turbulent channel flow. In Andre,J.C. *et al* (Eds) *Turbulent Shear Flows vol. 6 Springer, Berlin* , 85–96.

Kline, S.J. , Reynolds, W.C. Schraub, F.A. & Rustandler,P.W. 1967 The structure of turbulent boundary layers J. Fluid Mech**30**, 741–773.